Atmospheric correction of satellite ocean color imagery using the ultraviolet wavelength for highly turbid waters

Xianqiang He,[1*] Yan Bai,[1, 3] Delu Pan,[1] Junwu Tang,[2] and Difeng Wang [1]

[1]*State Key Laboratory of Satellite Ocean Environment Dynamics, Second Institute of Oceanography, State Oceanic Administration, Hangzhou, China*

[2]*National Ocean Technology Center, State Oceanic Administration, Tianjin, China*

[3]*Key Laboratory of Urban wetland and regional Variation Research of Zhejiang Province, Hangzhou Normal University, Hangzhou, China*

[*]*hexianqiang@sio.org.cn*

Abstract: Instead of the conventionally atmospheric correction algorithms using the near-infrared and shortwave infrared wavelengths, an alternative practical atmospheric correction algorithm using the ultraviolet wavelength for turbid waters (named UV-AC) is proposed for satellite ocean color imagery in the paper. The principle of the algorithm is based on the fact that the water-leaving radiance at ultraviolet wavelengths can be neglected as compared with that at the visible light wavelengths or even near-infrared wavelengths in most cases of highly turbid waters due to the strong absorption by detritus and colored dissolved organic matter. The UV-AC algorithm uses the ultraviolet band to estimate the aerosol scattering radiance empirically, and it does not need any assumption of the water's optical properties. Validations by both of the simulated data and in situ data show that the algorithm is appropriate for the retrieval of the water-leaving radiance in turbid waters. The UV-AC algorithm can be used for all the current satellite ocean color sensors, and it is especially useful for those ocean color sensors lacking the shortwave infrared bands. Moreover, the algorithm can be used for any turbid waters with negligible water-leaving radiance at ultraviolet wavelength. Based on our work, we recommend the future satellite ocean color remote sensors setting the ultraviolet band to perform the atmospheric correction in turbid waters.

OCIS codes: (010.0010) Atmospheric and oceanic optics; (010.1285) Atmospheric correction; (010.4450) Oceanic optics.

References and links

1. H. R. Gordon and M. Wang, "Retrieval of water-leaving radiance and aerosol optical thickness over the oceans with SeaWiFS: a preliminary algorithm," Appl. Opt. **33**(3), 443–452 (1994).
2. D. A. Siegel, M. Wang, S. Maritorena, and W. Robinson, "Atmospheric correction of satellite ocean color imagery: the black pixel assumption," Appl. Opt. **39**(21), 3582–3591 (2000).
3. K. G. Ruddick, F. Ovidio, and M. Rijkeboer, "Atmospheric correction of SeaWiFS imagery for turbid coastal and inland waters," Appl. Opt. **39**(6), 897–912 (2000).
4. C. Hu, K. L. Carder, and F. E. Muller-Karger, "Atmospheric correction of SeaWiFS imagery over turbid coastal waters: a practical method," Remote Sens. Environ. **74**(2), 195–206 (2000).
5. R. P. Stumpf, R. A. Arnone, R. W. Gould, P. M. Martinolich, and V. Ransibrahmanakul, "A partially coupled ocean-atmosphere model for retrieval of water-leaving radiance from SeaWiFS in coastal waters," SeaWiFS Postlaunch Tech. Rep. Ser., vol.22, NASA Tech. Memo. 2003–20682, S. B. Hooker and E. R. Firestone, eds., NASA Goddard Space Flight Center, Greenbelt, Maryland, pp. 51–59 (2003).
6. S. J. Lavender, M. H. Pinkerton, G. F. Moore, J. Aiken, and D. Blondeau-Patissier, "Modification to the atmospheric correction of SeaWiFS ocean colour images over turbid waters," Cont. Shelf Res. **25**(4), 539–555 (2005).
7. S. W. Bailey, B. A. Franz, and P. J. Werdell, "Estimation of near-infrared water-leaving reflectance for satellite ocean color data processing," Opt. Express **18**(7), 7521–7527 (2010).
8. M. Wang, W. Shi, and L. Jiang, "Atmospheric correction using near-infrared bands for satellite ocean color data processing in the turbid western Pacific region," Opt. Express **20**(2), 741–753 (2012).

#170576 - $15.00 USD Received 13 Jun 2012; revised 13 Aug 2012; accepted 14 Aug 2012; published 24 Aug 2012

9. M. Wang and W. Shi, "Estimation of ocean contribution at the MODIS near infrared wavelengths along the east coast of the U.S.: two case studies," Geophys. Res. Lett. **32**(13), L13606 (2005), doi:10.1029/2005GL022917.
10. M. Wang, "Remote sensing of the ocean contributions from ultraviolet to near-infrared using the shortwave infrared bands: simulations," Appl. Opt. **46**(9), 1535–1547 (2007).
11. M. Wang and W. Shi, "The NIR-SWIR combined atmospheric correction approach for MODIS ocean color data processing," Opt. Express **15**(24), 15722–15733 (2007).
12. M. Wang, S. Son, and W. Shi, "Evaluation of MODIS SWIR and NIR-SWIR atmospheric correction algorithm using SeaBASS data," Remote Sens. Environ. **113**(3), 635–644 (2009).
13. M. Wang, J. Tang, and W. Shi, "MODIS-derived ocean color products along the China east coastal region," Geophys. Res. Lett. **34**(6), L06611 (2007), doi:10.1029/2006GL028599.
14. W. Shi and M. Wang, "An assessment of the black ocean pixel assumption for MODIS SWIR bands," Remote Sens. Environ. **113**(8), 1587–1597 (2009).
15. M. Oo, M. Vargas, A. Gilerson, B. Gross, F. Moshary, and S. Ahmed, "Improving atmospheric correction for highly productive coastal waters using the short wave infrared retrieval algorithm with water-leaving reflectance constraints at 412 nm," Appl. Opt. **47**(21), 3846–3859 (2008).
16. X. Q. He, D. L. Pan, and Z. H. Mao, "Atmospheric correction of SeaWiFS imagery for turbid coastal and inland waters," Acta Oceanol. Sin. **23**(4), 609–615 (2004).
17. D. Doxaran, J. M. Froidefond, S. Lavender, and P. Castaing, "Spectral signature of highly turbid water application with SPOT data to quantify suspended particulate matter concentrations," Remote Sens. Environ. **81**(2), 149–161 (2002).
18. D. Doxaran, J. M. Froidefond, and P. Castaing, "Remote-sensing reflectance of turbid sediment-dominated waters. Reduction of sediment type variations and changing illumination conditions effects by use of reflectance ratios," Appl. Opt. **42**(15), 2623–2634 (2003).
19. IOCCG, "Ocean colour observations from a geostationary orbit," D. Antoine (Ed.), *Reports of the International Ocean-Colour Coordinating Group*, No.12, IOCCG, Dartmouth, Canada (2012).
20. M. Wang and H. R. Gordon, "Radiance reflected from the ocean-atmosphere system: synthesis from individual components of the aerosol size distribution," Appl. Opt. **33**(30), 7088–7095 (1994).
21. H. R. Gordon, J. W. Brown, and R. H. Evans, "Exact Rayleigh scattering calculations for use with the Nimbus-7 Coastal Zone Color Scanner," Appl. Opt. **27**(5), 862–871 (1988).
22. H. R. Gordon and M. Wang, "Surface-roughness considerations for atmospheric correction of ocean color sensors. I: The Rayleigh-scattering component," Appl. Opt. **31**(21), 4247–4260 (1992).
23. M. Wang and H. R. Gordon, "A simple, moderately accurate, atmospheric correction algorithm for SeaWiFS," Remote Sens. Environ. **50**(3), 231–239 (1994).
24. H. R. Gordon, "Atmospheric correction of ocean color imagery in the Earth Observing System era," J. Geophys. Res. **102**(D14), 17081–17106 (1997).
25. X. Q. He, D. L. Pan, Y. Bai, Q. K. Zhu, and F. Gong, "Evaluation of the aerosol models for SeaWiFS and MODIS by AERONET data over open oceans," Appl. Opt. **50**(22), 4353–4364 (2011).
26. D. L. Yuan, J. R. Zhu, C. Y. Li, and D. X. Hu, "Cross-shelf circulation in the Yellow and East China Seas indicated by MODIS satellite observations," J. Mar. Syst. **70**(1-2), 134–149 (2008).
27. M. Zhang, J. Tang, J. Dong, Q. Song, and J. Ding, "Retrieval of total suspended matter concentration in the Yellow and East China Seas from MODIS imagery," Remote Sens. Environ. **114**(2), 392–403 (2010).
28. J. H. Ryu, J. K. Choi, J. Eom, and J. H. Ahn, "Temporal variation in Korean coastal waters using Geostationary Ocean Color Imager," J. Coast. Res. **SI64**, 1731–1735 (2011).
29. X. Q. He, Y. Bai, D. L. Pan, N. L. Huang, X. Dong, J. S. Chen, and Q. F. Cui, "Using geostationary satellite ocean color data to map the diurnal dynamics of suspended particulate matter in coastal waters," Remote Sens. Environ. (to be published) (2012).
30. A. Morel and B. Gentili, "Diffuse reflectance of oceanic waters. II Bidirectional aspects," Appl. Opt. **32**(33), 6864–6879 (1993).
31. G. F. Moore, J. Aiken, and S. J. Lavender, "The atmospheric correction of water colour and quantitative retrieval of suspended particulate matter in Case II waters: application to MERIS," Int. J. Remote Sens. **20**(9), 1713–1733 (1999).
32. M. Doron, S. Bélanger, D. Doxaran, and M. Babin, "Spectral variations in the near-infrared ocean reflectance," Remote Sens. Environ. **115**(7), 1617–1631 (2011).

1. Introduction

Atmospheric correction is a key process for quantitative satellite ocean color remote sensing, which retrieves the desired water-leaving radiance and associated aerosol information from the sensor-measured radiance at the top-of-atmosphere (TOA). The concentrations of the upper ocean chlorophyll-a, suspended particulate matter, colored dissolved organic matter, and ocean optical properties can be computed from the water-leaving radiance retrieved by the atmospheric correction algorithm. These parameters are important for studying and understanding biological and biogeochemical processes, and monitoring global changes.

At satellite altitude, the total radiance received by ocean color sensor is the sum of the contributions mainly from the atmospheric molecules Rayleigh scattering, aerosol scattering,

#170576 - $15.00 USD Received 13 Jun 2012; revised 13 Aug 2012; accepted 14 Aug 2012; published 24 Aug 2012

sea surface reflectance and water-leaving radiance. The Rayleigh scattering and surface reflectance can be calculated accurately, and the priority problem of the atmospheric correction is the estimation of the aerosol scattering radiances. For clear water in the open ocean and continental shelf, the atmospheric correction scheme developed by Gordon and Wang (1994) [1] works quite well; it estimates the aerosol scattering radiances from two near-infrared (NIR) bands based on the assumption that the water-leaving radiances at these two NIR bands are negligible because of strong water absorption (black pixel assumption). However, in turbid coastal waters, this scheme tends to overestimate the aerosol scattering radiance and thus underestimate the water-leaving radiance, because of the significant contribution of the water-leaving radiance at NIR and the failure of the black pixel assumption. To employ this scheme for turbid waters, several methods have been proposed to estimate and remove the contribution of the water-leaving radiance at NIR. Siegel et al. (2000) [2] estimated the water-leaving radiance at NIR through iteration with the retrieved chlorophyll-a concentration. Ruddick et al. (2000) [3] used the aerosol scattering reflectance ratio and water-leaving reflectance ratio between two NIR bands to analytically solve for the water-leaving reflectance and aerosol scattering reflectance at NIR simultaneously. Hu et al. (2000) [4] approximately applied the aerosol scattering reflectance at NIR estimated from the clear water pixels nearest the turbid waters. Stumpf et al. (2003) [5] used a bio-optical model of absorption coefficient in the red light band, and combined it with the water-leaving radiance in the red light band to estimate the water-leaving radiance at NIR. Lavender et al. (2005) [6] used the retrieved suspended particulate matter concentration to estimate the water-leaving radiance at NIR. Bailey et al. (2010) [7] improved the method proposed by Stumpf et al. (2003) [5] by applying optical models to compute the water-leaving radiance from the absorption coefficient in the red light band. Wang et al. (2012) [8] proposed an iterative scheme to estimate the water-leaving radiance at NIR using a regional relationship between the normalized water-leaving radiance at NIR and diffuse attenuation coefficient at 490nm, derived from long-term measurements with the MODIS (Moderate-resolution Imaging Spectroradiometer) in the western Pacific. A more appropriate approach has been proposed by Wang et al. in recent years [9–14], using two shortwave infrared (SWIR) bands instead of two NIR bands to estimate the aerosol scattering radiances in highly turbid waters, based on the fact that the water-leaving radiance at the SWIR is always negligible because of the much stronger water absorption. However, owing to the longer extrapolation wavelength distance from SWIR bands to the visible light bands, the SWIR algorithm is more sensitive to the aerosol models, especially for the absorption aerosol conditions [15]. To reduce the errors caused by the wrong selection of aerosol models based on the SWIR bands, Oo et al. (2008) [15] proposed a method to constrain the selection of aerosol models using the 412nm band for highly productive waters. Except for the SWIR algorithm, all of these methods are strongly dependent on the local water's optical properties or even the aerosol's properties. However, in coastal waters with strong tidal dynamics, terrestrial inputs and affected by anthropocentric aerosols, the water and aerosol's optical properties are very complex and highly heterogeneous, which will limit the applicability of the above methods.

Our motivation for this work is to propose an alternative practical algorithm using the ultraviolet wavelength (named UV-AC) to carry out the atmospheric correction for satellite ocean color data in highly turbid waters, especially for those satellites lacking the SWIR band, such as SeaWiFS (Sea-viewing Wide Field-of-view Sensor), MERIS (Medium Resolution Imaging Spectrometer), GOCI (Geostationary Ocean Color Imager), etc. In this paper, we first give the principle and algorithm for this practical atmospheric correction method in section 2. Then, we validate the UV-AC algorithm in section 3. Finally, we apply this algorithm to satellite data and validate the results with in situ data in section 4.

2. Atmospheric correction algorithm using ultraviolet wavelength

In the previous studies, we found that the water-leaving radiance (L_w) at the UV band was much less than that at the VIS or even NIR in China's east coast region, and thus we preliminarily proposed an atmospheric correction for SeaWiFS using the UV band for turbid

#170576 - $15.00 USD Received 13 Jun 2012; revised 13 Aug 2012; accepted 14 Aug 2012; published 24 Aug 2012

coastal and inland waters [16]. Actually, in turbid coastal waters, high concentrations of suspended particulate matter and colored dissolved organic matter (CDOM) generally dominate the water's optical properties. Due to strong particle scattering, L_w greatly increases in the VIS and NIR. Meanwhile, the strong absorption of detritus and CDOM cause a significant low L_w in the blue part of the VIS and even lower L_w in the UV, due to the exponential increase of the absorption coefficient with decrease of wavelength for detritus and CDOM. Figure 1 shows the examples of normalized water-leaving radiance (L_{wn}) measured in the estuaries of the Changjiang River, Mississippi River and Orinoco River. Clearly, L_{wn} at the VIS and NIR increases rapidly with the increase of water turbidity, but it increases very little at the UV. Even for the extremely turbid waters at the Changjiang River Estuary with a maximum up to 10.0 mW/(cm^2·μm·sr), L_{wn} at the UV is still less than 1.0 mW/(cm^2·μm·sr) and much less than that at the NIR (Fig. 1(b)). Moreover, Oo et al. (2008) [15] found that $L_{wn}(412nm)$ is relatively low and stable in the Chesapeake region, and thus they used 412 nm band to constrain the aerosol model selection for the SWIR-AC algorithm. In the Gironde Estuary in the southwest France, it was found that the remote sensing reflectance at 400 nm was quite smaller as compared to visible or even NIR [17,18]. Therefore, in most cases of the highly turbid waters, L_{wn} at the UV band can be neglected compared with that at the VIS and even NIR, and we can use the UV band to estimate aerosol scattering radiance. In some extremely turbid waters, L_{wn} at UV band may be much less than that at the NIR. For such cases, UV band is better than NIR band to obtain a more accurate atmospheric correction [19].

Although the above principle is easy to understand, it still needs some empirical techniques to implement the atmospheric correction algorithm using the UV band. Unlike the conventional atmospheric correction algorithms using two bands at NIR or SWIR to determine the suitable aerosol models (named NIR-AC and SWIR-AC, respectively), the UV-AC cannot use the same scheme with two UV bands due to the small wavelength distance between them. Here, we propose a practical algorithm to complete the atmospheric correction using the UV band for turbid waters.

The total reflectance (ρ_t) measured by an ocean color satellite sensor can be written as [20]

$$\rho_t(\lambda) = \rho_r(\lambda) + \rho_a(\lambda) + t_v(\lambda)\rho_w(\lambda), \quad (1)$$

where ρ_r is the Rayleigh-scattering reflectance by air molecules in the absence of aerosols; ρ_a is the aerosols multiple-scattering reflectance, including the interactive scattering between molecules and aerosol; ρ_w is the desired water-leaving reflectance; and t_v is the atmospheric diffuse transmittance from sea surface to the satellite. Note that in the Eq. (1), we ignore the sea surface reflectance from whitecaps and sun-glint. With Lambertian diffuser assumption for upward radiance, the definition of the reflectance in Eq. (1) is

$$\rho = \pi L / (F_0 \cos\theta_0), \quad (2)$$

where L is the upward radiance; F_0 is the extraterrestrial solar irradiance, and θ_0 is the solar zenith angle. The purpose of the atmospheric correction is to retrieve ρ_w from ρ_t. The Rayleigh-scattering component ρ_r can be accurately calculated using the atmospheric vector radiative transfer model with the knowledge of the atmosphere pressure and wind speed at the sea surface [21,22]. The aerosol, however, is highly variable, and the component ρ_a cannot be predicted a priori. The details for the estimation of ρ_a using the UV band are as followings:

#170576 - $15.00 USD Received 13 Jun 2012; revised 13 Aug 2012; accepted 14 Aug 2012; published 24 Aug 2012

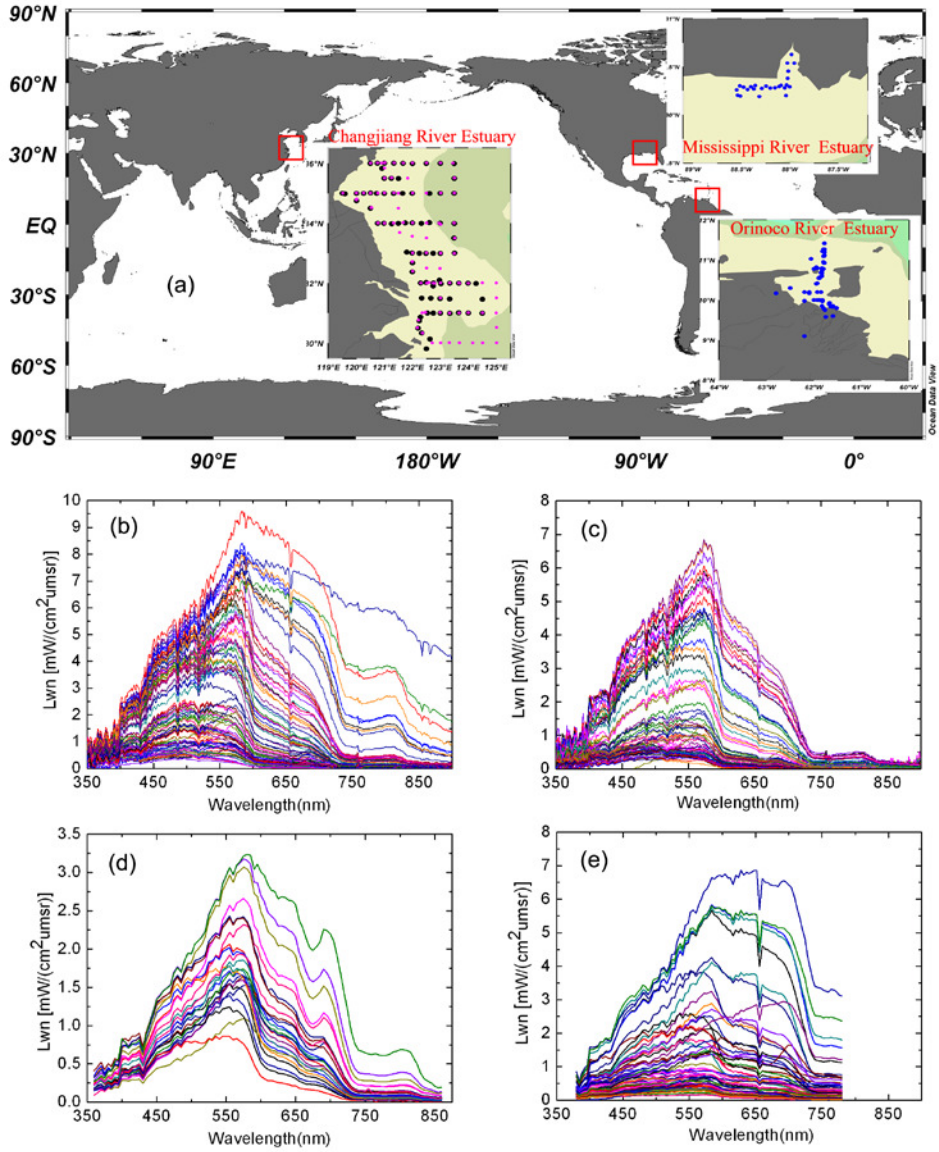

Fig. 1. Normalized water-leaving radiance (Lwn) measured in the Changjiang River Estuary, Mississippi River Estuary and Orinoco River Estuary. (a) Location of the sampling stations, with pink and black circles in the Changjiang River Estuary represent stations of spring and autumn cruises, respectively; (b) Lwn at Changjiang River Estuary in spring of 2003; (c) Lwn at Changjiang River Estuary in autumn of 2003; (d) Lwn at Mississippi River Estuary; (e) Lwn at Orinoco River Estuary. The above-water methods are used to measure the Lwn. The remote sensing reflectance data sets at Mississippi River Estuary and Orinoco River Estuary were downloaded from the SeaBASS, and were converted to Lwn by multiplying the mean extraterrestrial solar irradiance.

(1) Calculating the Rayleigh-scattering corrected reflectance for all bands as

$$\rho_{rc}(\lambda) = \rho_t(\lambda) - \rho_r(\lambda) = \rho_a(\lambda) + t_v(\lambda)\rho_w(\lambda); \quad (3)$$

(2) Assuming ρ_w at the UV band can be neglected due to the strong absorptions by terrestrial detritus and CDOM in turbid coastal waters (Fig. 1), we get the aerosol multiple-scattering

#170576 - $15.00 USD Received 13 Jun 2012; revised 13 Aug 2012; accepted 14 Aug 2012; published 24 Aug 2012

reflectance at the UV band with $\rho_a^{(e)}(UV) = \rho_{rc}(UV)$. In the following text, the superscript "(e)" means the estimated value instead of the actual value;

(3) Estimating the aerosol scattering reflectance at the longer NIR band (NIR_L) using the moderate accuracy extrapolation model for aerosol scattering reflectance developed by Wang and Gordon (1994) [23], as

$$\rho_a^{(e)}(NIR_L) = \rho_a^{(e)}(UV)\left[\varepsilon_{(NIR_S,NIR_L)}^{(e)}\right]^{-(NIR_L-UV)/(NIR_L-NIR_S)}, \quad (4)$$

where $\varepsilon_{(NIR_S,NIR_L)}^{(e)}$ is the ratio of $\rho_{rc}(\lambda)$ at two NIR bands, that is, $\varepsilon_{(NIR_S,NIR_L)}^{e} = \rho_{rc}(NIR_S)/\rho_{rc}(NIR_L)$ with NIR_S for shorter NIR and NIR_L for longer NIR. In the following text, ε is defined as the aerosol multiple-scattering epsilon.

Gordon (1997) [24] pointed out that for non- and weakly absorption aerosol (maritime, coastal, and tropospheric aerosol models), the performance of the extrapolation model of Eq. (4) was truly remarkable, and the retrieved value of normalized water-leaving reflectance was usually within the acceptable limits. Also, the Eq. (4) with aerosol multiple-scattering epsilon was used by Ruddick et al. (2000) [3] to analysis the error in water-leaving reflectance retrieval caused by the multiple-scattering epsilon uncertainty. Therefore, Eq. (4) can be used to extrapolate the aerosol multiple-scattering reflectance to different wavelength.

Our UV-AC algorithm is specially design for the turbid coastal waters. In the practical processing for satellite images, it does not need to strictly separate the turbid water and clear water. When encounter the clear water nearby the desired turbid water, our method will use the near infrared band instead of the UV band by limit the $\rho_a^{(e)}(NIR_L)$ to $\rho_{rc}(NIR_L)$. Of course, if one only focuses for the clear water, it is recommended to use the near infrared wavelengths based method.

(4) Assuming the spectrum of the aerosol scattering reflectance is "white" (or flat), then the aerosol scattering reflectance at all bands is equal to $\rho_a^{(e)}(NIR_L)$.

The critical point for the UV-AC algorithm is the rationality of the empirical estimation of the aerosol multiple-scattering reflectance at NIR_L ($\rho_a^{(e)}(NIR_L)$) by $\rho_a^{(e)}(UV)$ according to Eq. (4). We call the "empirical estimation" because both the $\rho_a^{(e)}(UV)$ and $\varepsilon_{(NIR_S,NIR_L)}^{(e)}$ inputted into the moderate accuracy extrapolation model (Eq. (4)) are approximately estimated values instead of the actual values. First, $\rho_a^{(e)}(UV)$ is always larger than the actual value $\rho_a(UV)$ due to the contribution of water-leaving radiance, though the water-leaving reflectance is small at the UV in turbid waters. Second, $\varepsilon_{(NIR_S,NIR_L)}^{(e)}$ is generally larger than the real value of the ratio of aerosol multiple-scattering reflectance at two NIR bands ($\varepsilon_{(NIR_S,NIR_L)} = \rho_a(NIR_S)/\rho_a(NIR_L)$. For evidence please refer to Appendix A). Therefore, $\rho_a^{(e)}(UV)$ would tend to overestimate the aerosol scattering reflectance at NIR_L, but on the contrary, $\varepsilon_{(NIR_S,NIR_L)}^{(e)}$ would cause the underestimation. Thus, the compensating effect between $\rho_a^{(e)}(UV)$ and $\varepsilon_{(NIR_S,NIR_L)}^{(e)}$ is expected to get a more reasonable estimation of the aerosol scattering reflectance at NIR_L. It needs to note that the UV-AC algorithm assumes the spectrally flat reflectance for aerosols (or "white" aerosol). Generally, the "white" aerosol approximation is rationale for the coastal aerosol models and maritime aerosol models, which are the dominating aerosol types in the coastal regions [1]. While for the tropospheric aerosol models, the "white" aerosol approximation may have large extrapolation error at the short

#170576 - $15.00 USD Received 13 Jun 2012; revised 13 Aug 2012; accepted 14 Aug 2012; published 24 Aug 2012

wavelengths [1]. Since the UV-AC algorithm mainly focuses on the atmospheric correction in coastal regions, the impact of tropospheric aerosol is expected to be small.

3. Validation of the UV-AC algorithm

We theoretically deduced the error of the water-leaving radiance (including the atmospheric diffuse transmittance) at the VIS ($t_v^{VIS} L_w^{VIS}$) retrieved by the UV-AC algorithm, and the result showed that the error of $t_v^{VIS} L_w^{VIS}$ was generally larger than $-\left[F_0(VIS)/F_0(UV)\right]t_v(UV)L_w(UV)$, and less than $\left[F_0(VIS)/F_0(UV)\right]L_a(UV)$ (for evidence please refer to Appendix B). From Fig. 1, we can see that the average value of $L_{wn}(UV)$ is about 0.5 mW/(cm^2·μm·sr). Also, for a clear to moderately turbid atmosphere, $L_a(UV)$ is generally less than 0.5 mW/(cm^2·μm·sr) for zenith viewing. Therefore, for most cases, the retrieval error of the water-leaving radiance by the UV-AC algorithm is expected to be less than 1.0 mW/(cm^2·μm·sr).

Furthermore, we simulated the Rayleigh-scattering corrected reflectance at nine wavelengths (365, 412, 443, 490, 510, 555, 670, 765 and 865 nm) using Eq. (3), to validate the performance of the UV-AC algorithm. First, the water-leaving reflectance (ρ_w) was estimated with the in situ measured L_{wn} for turbid waters with $L_{wn}(555nm)$ larger than 2.0 mW/(cm^2·μm·sr). As shown in Figs. 1(b)-1(e), there are no values at 365 nm and 865 nm for the L_{wn} measured in the Orinoco River Estuary, here we only used the L_{wn} measured in the Changjiang River Estuary and Mississippi River Estuary, and there are 76 effective samples with $L_{wn}(555nm) \geq 2.0$ mW/(cm^2·μm·sr). Then, for each sample, we simulated the aerosol scattering reflectance and atmospheric diffuse transmittance for different aerosol models and solar-satellite geometries. All the twelve aerosol models defined for SeaWiFS and MODIS in the SeaDAS (SeaWiFS Data Analysis System) version 5.3 were used in the simulation. These twelve aerosol models include the Oceanic model with relative humidity (RH) of 99% (O99), the Maritime model with RH of 50%, 70%, 90% and 99% (M50, M70, M90 and M99), the Coastal model with RH of 50%, 70%, 90% and 99% (C50, C70, C90 and C99) and the Tropospheric model with RH of 50%, 90% and 99% (T50, T90 and T99) [25]. In the simulation, the inputted aerosol multiple-scattering reflectance at 865nm is varying from 0.004 to 0.012 with steps of 0.004, the solar and satellite zenith angles varying from 0° to 60° with step of 30°, and the solar-satellite relative azimuth angles varying from 0° to 120° with step of 60°. Then, for each aerosol model and specific user-inputted aerosol multiple-scattering reflectance at 865 nm and solar-satellite geometries, we calculated the aerosol single-scattering reflectance at 865 nm according to the aerosol scattering look-up tables taken from the SeaDAS, and then the aerosol single-scattering reflectance at other eight wavelengths were extrapolated from 865 nm. Finally, the multiple-scattering reflectances at all wavelengths were calculated by the single-scattering reflectance using the aerosol scattering look-up tables. Here the extrapolation method is the same as that used in the SeaDAS, and for the details readers can refer to [1]. Since there were no look-up tables for 365 nm in the SeaDAS, we extrapolated the aerosol scattering reflectance and atmospheric diffuse transmittance to 365 nm using the spline interpolation method. Finally, we have a simulated data set of the Rayleigh-scattering corrected reflectance for the validation in the next step, with total 73872 samples covering all twelve aerosol models and the general variation ranges of the aerosol scattering reflectance and solar-satellite geometries. Figure 2 shows an example of the simulated aerosol multiple-scattering reflectance for solar and satellite zenith angles of 30°, relative azimuth angle of 120°, and aerosol multiple-scattering reflectance at 865nm of 0.008. It can be seen that "white" aerosol approximation is rationale for the coastal aerosol models and maritime aerosol models, which are the dominating aerosol types in the coastal regions [1]. We have quantified the extrapolation error for 412 nm band by using the aerosol multiple-scattering reflectance at 443 nm and longer wavelengths for all

#170576 - $15.00 USD Received 13 Jun 2012; revised 13 Aug 2012; accepted 14 Aug 2012; published 24 Aug 2012

the simulated samples, and the results showed that the mean absolute relative error caused by extrapolation was 0.7% in logarithmic scale. Therefore, the error caused by extrapolation method is quite small.

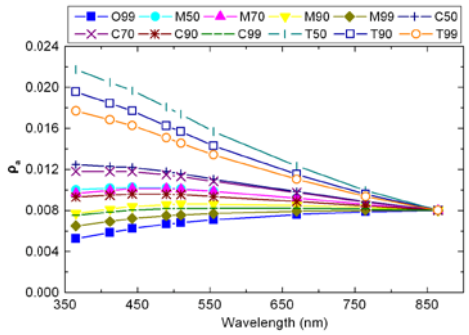

Fig. 2. Simulated aerosol multiple-scattering reflectance for solar and satellite zenith angles of 30°, relative azimuth angle of 120°, and aerosol multiple-scattering reflectance at 865nm of 0.008. Individual curves mean the 12 aerosol models from SeaDAS.

We applied the UV-AC algorithm based on 365nm (named UV-AC(365nm)) to the simulated Rayleigh-scattering corrected reflectance, and retrieved the water-leaving reflectance (including the atmospheric diffuse transmittance). Figure 3(a) shows the comparison of the water-leaving reflectance between the UV-AC(365nm) retrieved value and in situ measurement. Although the UV-AC(365nm) slightly overestimated the water-leaving reflectance as a whole, the retrieved water-leaving reflectance agreed quite well with the in situ values, especially at the longer wavelengths. The correlation coefficients are 0.64, 0.76, 0.86, 0.90, 0.95, 0.99, 0.98, and 0.98 for the 412, 443, 490, 510, 555, 670, 765 and 865 nm, respectively. Therefore, for most cases, UV-AC(365nm) can retrieve the water-leaving reflectance well.

In some cases of extremely turbid waters, UV-AC(365nm) may underestimate the water-leaving reflectance, as the points in the red ellipse in Fig. 3(a), which correspond to the same sample with maximal $L_{wn}(865nm)$ in Fig. 1(b). Actually, the in situ suspended particulate matter concentration (SPM) at this sampling station was up to 1649.9 mg/l. The major reason is the overestimation of aerosol scattering reflectance at 865 nm by the UV-AC(365nm). Specifically, from the clear shelf water to the turbid coastal water, $\varepsilon^{(e)}_{(NIR_S,NIR_L)}$ first increases with the increase of water turbidity, and it reaches the maximum value at a certain turbidity (e.g. SPM is around 100-200 mg/l), then it decreases with the further increase of water turbidity (for details, please refer to Appendix A). Therefore, in the extremely turbid waters, $\varepsilon^{(e)}_{(NIR_S,NIR_L)}$ is much lower than that in the moderately turbid waters. According to the Eq. (4), the decrease of $\varepsilon^{(e)}_{(NIR_S,NIR_L)}$ will increase the aerosol scattering reflectance at the NIR, which will induce the overestimation of the aerosol scattering reflectance at 865 nm.

Past and current on-orbit satellite ocean color sensors, such as SeaWiFS, MODIS and MERIS, have no UV band, and their shortest wavelength is 412 nm. Here, we use the same scheme as the UV-AC(365nm) algorithm but take 412 nm as the reference band (named UV-AC(412nm)). Interestingly, though the larger water-leaving radiance at 412 nm as compared with 365 nm (Fig. 1), the performance of the UV-AC(412nm) is very similar as the UV-AC(365nm), with the correlation coefficients of 0.59, 0.72, 0.84, 0.89, 0.95, 0.99, 0.97, 0.97 for the 412, 443, 490, 510, 555, 670, 765 and 865 nm, respectively (Fig. 3(b)). Moreover, the UV-AC(412nm) can slightly reduce the overestimation of the water-leaving reflectance compared with the UV-AC(365nm). However, the UV-AC(412nm) significantly underestimates the water-leaving reflectance for extremely turbid waters as the points in the

#170576 - $15.00 USD Received 13 Jun 2012; revised 13 Aug 2012; accepted 14 Aug 2012; published 24 Aug 2012

red ellipse in Fig. 3(b), which correspond to the same sample with maximal $L_{wn}(865nm)$ in Fig. 1(b).

As a whole, both the UV-AC(365nm) and UV-AC(412nm) can reproduce the spectral distribution of the in situ water-leaving reflectance with similar mean value and standard deviation (Fig. 3(c)). For the UV-AC(365nm) algorithm, the retrieved mean value and standard deviation of the water-leaving reflectance agrees very well with the in situ value at longer wavelengths, indicating the good performance of the UV-AC(365nm) for the estimation of aerosol scattering reflectance at 865 nm. Yet, the overestimation of water-leaving reflectance at short visible wavelengths indicates that the reason of the overestimation may due to the underestimation of aerosol scattering reflectance by the assumption of the "white" aerosol. Compared with the UV-AC(365nm), UV-AC(412nm) slightly overestimates the aerosol scattering reflectance at 865 nm due to the larger contribution of water-leaving radiance at 412 nm. However, the overestimation of the aerosol scattering reflectance at 865 nm can compensate the slight overestimation caused by the "white" aerosol assumption for the short visible wavelengths, as shown in Fig. 3(c).

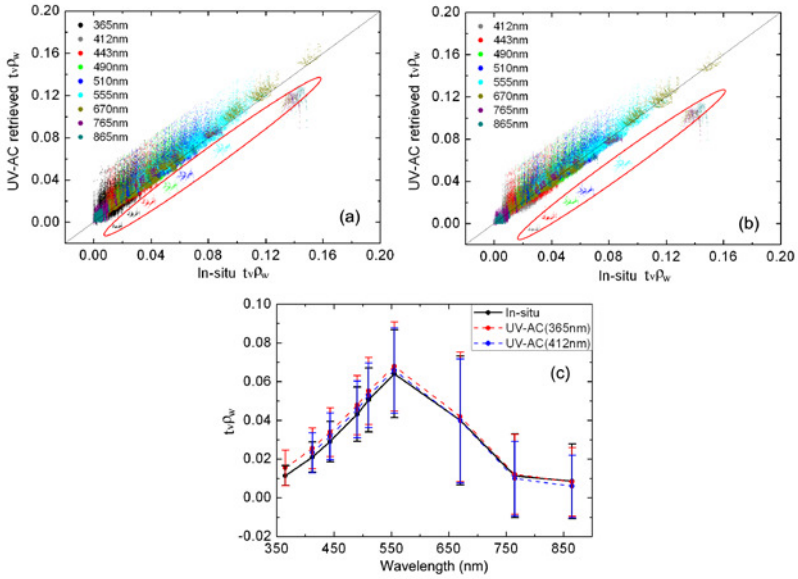

Fig. 3. Comparison of the water-leaving reflectance retrieved by the UV-AC algorithms and the in situ measured water-leaving reflectance. (a) scatter plot for the UV-AC algorithm based on 365nm; (b) scatter plot for the UV-AC algorithm based on 412nm; (c) spectral distributions of the mean value and standard deviation of water-leaving reflectance. Points in the red ellipses in (a) and (b) correspond to the same sample with maximal $L_{wn}(865nm)$ shown in Fig. 1(b).

4. Application of the UV-AC algorithm to satellite data

To examine the performance of the UV-AC algorithm for the real satellite data, we applied the UV-AC(412nm) algorithm to the Aqua/MODIS data on 5 April 2003, and retrieved the L_{wn} in the Changjiang River Estuary, as shown in Fig. 4. Since the ocean color bands of Aqua/MODIS saturated in highly turbid coastal waters, there were no effective values in the coasts. Clearly, L_{wn} decreased with the increase of distance offshore, as expected. Also, moving with the southeast Subei Coastal Current, the turbid water from the Subei Shallow intruded onto the continental shelf. This intrusion phenomenon has already been analyzed by Yuan et al. (2008) [26] using the monthly-averaged normalized water-leaving radiance of Terra/MODIS at 551 nm combined with in situ hydrographic and current measurements. Off

#170576 - $15.00 USD Received 13 Jun 2012; revised 13 Aug 2012; accepted 14 Aug 2012; published 24 Aug 2012

the mouth of the Changjiang River, the clear water from the continental shelf intruded into the Subei Shallow driven by the northward Taiwan Warm Current. So, the L_{wn} retrieved by UV-AC algorithm reflected the local hydrodynamics quite well.

More importantly, the L_{wn} retrieved by the UV-AC algorithm is always positive, even for the extremely turbid waters. As a comparison, we also processed Aqua/MODIS data on 5 April 2003 using the SeaDAS (version 6.3), and retrieved the normalized water-leaving radiance by applying the combined SWIR and NIR atmospheric correction algorithm (named SWIR/NIR-AC), as shown in Fig. 5. Obviously, the SWIR/NIR-AC algorithm significantly underestimated the normalized water-leaving radiance especially at short visible wavelengths, and got the negative water-leaving radiance at 412nm for almost the whole region. Generally speaking, $L_{wn}(551nm)$ generally increases with the water turbidity; but, near the coast of the Subei Shallow with extreme turbidity, the normalized water-leaving radiances retrieved by the SWIR/NIR-AC algorithm were much lower than the surrounding shelf waters, which was not in accord with the facts.

We further compared the satellite-retrieved L_{wn} with the in situ measurements in the Changjiang River Estuary. In April 2003, a cruise was carried out in the Changjiang River Estuary, as shown in Fig. 1(a). For the details of the cruise and the measurement method for water-leaving radiance, readers should refer to Zhang et al. (2010) [27]. During the cruise, only four stations named HD34 (123.49639°E, 32.98528°N), HD35 (123.00472°E, 32.99194°N), HD36 (122.50083°E, 33.00500°N) and HD37 (122.00556°E, 33.00056°N) were measured on 5 April 2003 (Fig. 6(a)). Figures 6(b)-6(e) show the comparisons between the satellite-derived normalized water-leaving radiances retrieved by the UV-AC and SWIR/NIR-AC algorithms and the in situ measurements at each station. As a whole, the L_{wn} retrieved by the UV-AC algorithm matched the in situ measurements very well in both values and spectral shapes. However, the SWIR/NIR-AC algorithm significantly underestimates the normalized water-leaving radiances, and even got negative values at short visible wavelengths. It needs to be noted that we ignore the diurnal variation of the normalized water-leaving radiance between the time difference of the in situ measurement and satellite observation. Since all four stations are located at the middle shelf, the diurnal variations are expected to be small.

Furthermore, we applied the UV-AC algorithm to GOCI data to examine the stability of algorithm performance in the turbid coastal waters. GOCI is the world's first ocean color imager in geostationary orbit, launched on 27 June 2010 by South Korea. Compared with other satellite ocean color sensors, GOCI has a unique capability to monitor short term and regional oceanic phenomena (tide dynamic, red tides, river plume, sediment transport and etc.) with high spatial resolution (500 m) and very high temporal resolution (1 hour), which makes it very useful for monitoring the diurnal dynamics of material in coastal areas. GOCI has 8 visible-to-near-infrared bands (412, 443, 490, 555, 660, 680, 745 and 865 nm) with high signal-noise ratios, enabling more accurate retrieval of ocean color information. The observing area of GOCI is about 2500km × 2500km (116.08°E~143.92°E, 24.75°N~47.25°N for central directions) centered on 130°E and 36°N, covering the coasts of East China, the Korean peninsula, Japan, and their corresponding shelves and open oceans [28].

#170576 - $15.00 USD Received 13 Jun 2012; revised 13 Aug 2012; accepted 14 Aug 2012; published 24 Aug 2012

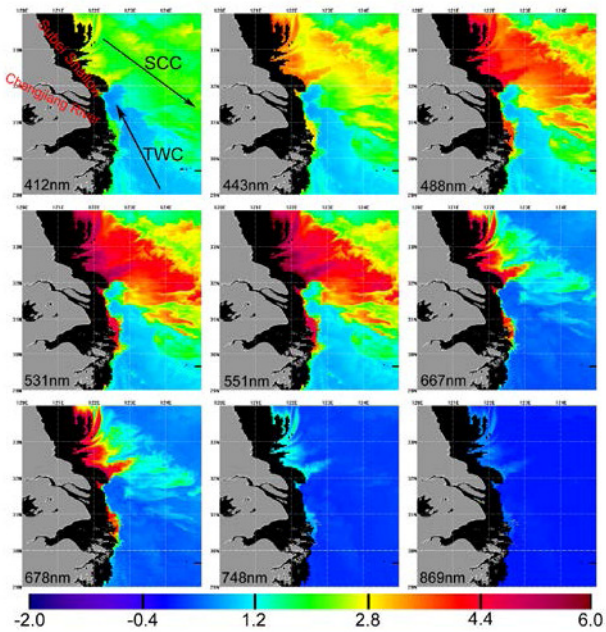

Fig. 4. The L_{wn} retrieved by Aqua/MODIS on 5 April 2003 using the UV-AC(412nm) algorithm (unit: mW/(cm^2·μm·sr)). Arrows in the sub-image of 412nm indicate the Subei Coastal Current (SCC) and the Taiwan Warm Current (TWC).

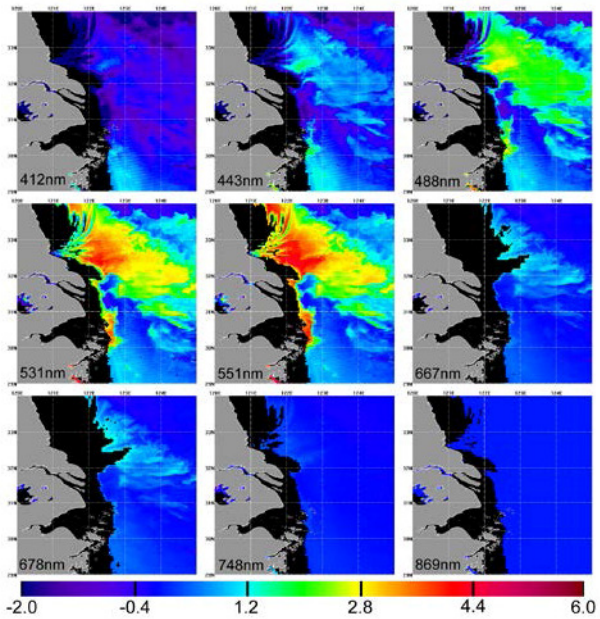

Fig. 5. The L_{wn} retrieved by Aqua/MODIS on 5 April 2003 using the SeaDAS 6.3 based on the SWIR/NIR-AC algorithm (unit: mW/(cm^2·μm·sr)).

#170576 - $15.00 USD Received 13 Jun 2012; revised 13 Aug 2012; accepted 14 Aug 2012; published 24 Aug 2012

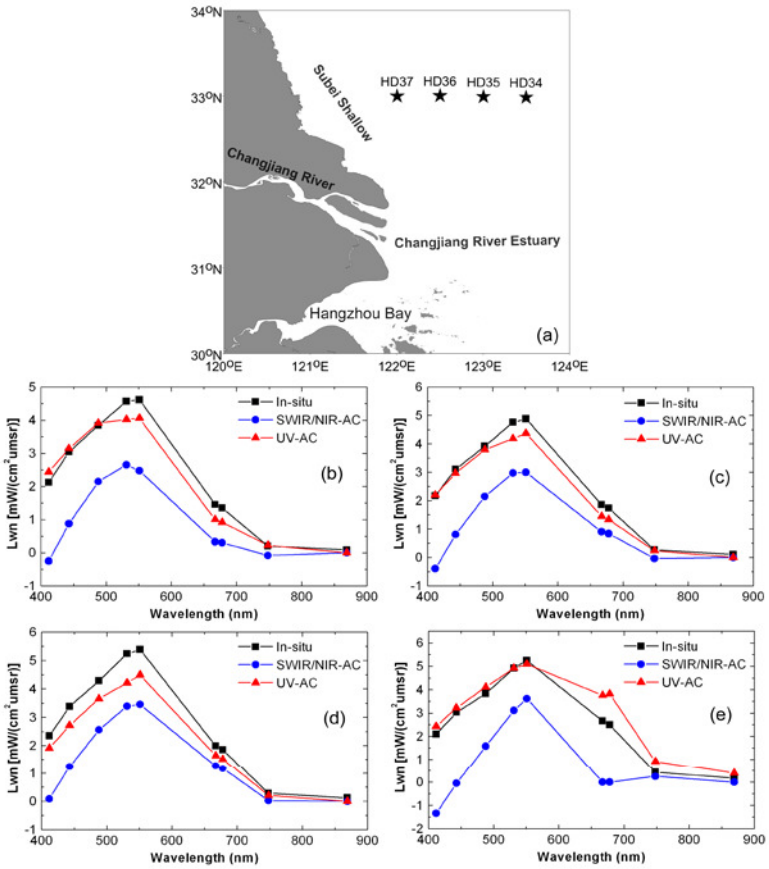

Fig. 6. Comparisons between satellite retrieved and in situ measured normalized water-leaving radiances. (a) Locations of the in situ measurement of normalized water-leaving radiances on 5 April 2003 (marked as stars); (b) comparison at station HD34; (c) comparison at station HD35; (d) comparison at station HD36; (e) comparison at station HD37.

For each day, GOCI observes 8 times from midmorning to midafternoon (8:28-15:28 Beijing time) with a step of 1 hour. Due to the variations of the solar zenith angle and aerosol conditions during the 8 observations in one day, GOCI data is an ideal satellite data set for examining the stability of the atmospheric correction algorithm. Here, we applied the UV-AC(412nm) algorithm to GOCI data on 5 April 2011, and retrieved the L_{wn} at 8 observations. Figure 7(a)-7(h) show examples of the retrieved $L_{wn}(660nm)$ for all 8 observations. Clearly, for inland waters (such as in Lake Taihu and the inner Changjiang River) and middle shelf waters, the variations of the retrieved normalized water-leaving radiances among the 8 observations were very small. Furthermore, we selected a section covering the clear, turbid and extremely turbid waters as the line AB in the Fig. 7(a), to examine the stability of algorithm performance. Figure 7(i) shows the comparison of the $L_{wn}(660nm)$ at 8 observing times along the section AB. As a whole, the GOCI-retrieved $L_{wn}(660nm)$ at all 8 observing times are consistence with each other quite well, indicating the stability of the performance of the UV-AC algorithm. For the areas affected by the strong tides such as the extremely turbid waters in the Changjiang River Estuary and Hangzhou Bay, they had significantly diurnal dynamics as revealed by the variations of the GOCI-retrieved $L_{wn}(660nm)$, and we have analyzed such diurnal dynamics using the GOCI data in another paper [29].

#170576 - $15.00 USD Received 13 Jun 2012; revised 13 Aug 2012; accepted 14 Aug 2012; published 24 Aug 2012

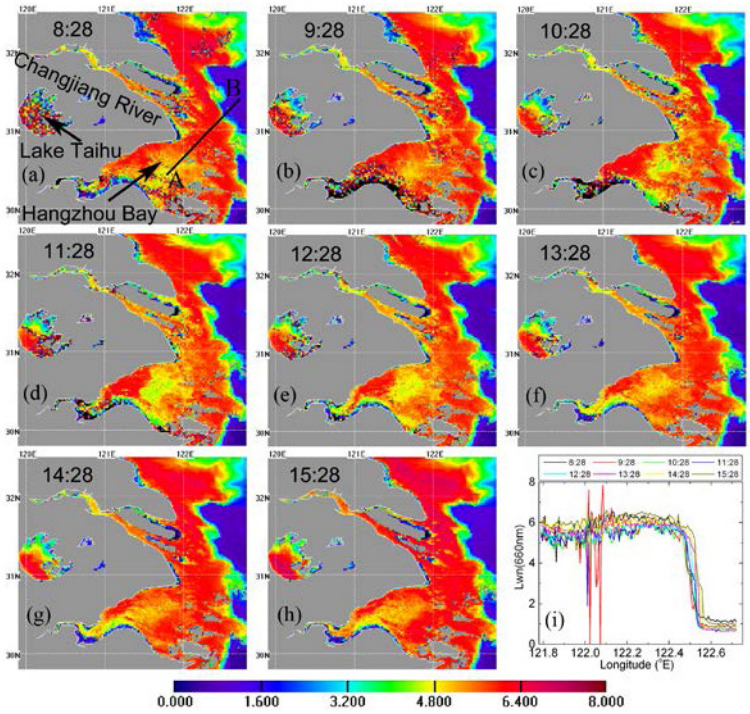

Fig. 7. GOCI-retrieved $L_{wn}(660nm)$ (unit: mW/(cm^2·μm·sr)) using the UV-AC(412nm) algorithm on 5 April 2011. The time labels on (a)-(h) are the corresponding observing time in Beijing time. (i) is the comparison of $L_{wn}(660nm)$ along the section AB in the sub-image (a).

5. Conclusion

In this paper, we propose an atmospheric correction algorithm using the UV band for turbid waters. The algorithm is practical and valid for the retrieval of water-leaving radiance at the wavelengths of VIS and NIR. Therefore, it is very useful for the retrieval of the suspended particulate matter concentration and the chlorophyll fluorescence in turbid coastal waters. For blue part of VIS, the UV-AC algorithm slightly overestimates the water-leaving radiance due to the "white" aerosol assumption. The major disadvantage of the UV-AC algorithm is the assumption of the negligible water-leaving radiance at the UV band that is important for the retrieval of CDOM. However, these problems can be solved by using a three step method. First, we can take the inverse of the suspended particulate matter concentration by using the water-leaving radiance retrieved by the UV-AC algorithm. Second, we estimate the water-leaving radiance at the two NIR bands based on the retrieved suspended particulate matter concentration. Third, we can directly use the standard atmospheric correction algorithm using the two NIR bands corrected by the estimated water-leaving radiances.

The UV-AC algorithm needs the assumption that water-leaving radiance at ultraviolet wavelength can be neglected as compared with that at the visible or even near-infrared wavelengths. Such assumption is expected to be reasonable for mostly turbid coastal waters as examples shown in Fig. 1, while the general rationale of this assumption needs to be further validated by more in situ data in the future. Meanwhile, although we have validated the performance of the UV-AC algorithm for the general variation ranges of the aerosol and solar-satellite geometries, more in situ validations are needed for application of the UV-AC algorithm to different coastal waters. We recommend that future satellite ocean color remote

#170576 - $15.00 USD Received 13 Jun 2012; revised 13 Aug 2012; accepted 14 Aug 2012; published 24 Aug 2012

sensors set with the UV band be used to help with the atmospheric correction in turbid coastal waters, especially for satellites designed for monitoring coastal waters.

Appendix A: variation of $\varepsilon^{(e)}_{(NIR_S,NIR_L)}$ with water turbidity

We define $\alpha_{(NIR_S,NIR_L)}$ as

$$\alpha_{(NIR_S,NIR_L)} = \frac{t_v(NIR_S)\rho_w(NIR_S)}{t_v(NIR_L)\rho_w(NIR_L)}. \tag{5}$$

According to the definitions of $\varepsilon_{(NIR_S,NIR_L)}$ and $\varepsilon^{(e)}_{(NIR_S,NIR_L)}$ as

$$\begin{cases} \varepsilon_{(NIR_S,NIR_L)} = \dfrac{\rho_a(NIR_S)}{\rho_a(NIR_L)} \\ \varepsilon^{(e)}_{(NIR_S,NIR_L)} = \dfrac{\rho_{rc}(NIR_S)}{\rho_{rc}(NIR_L)} = \dfrac{\rho_a(NIR_S)+t_v(NIR_S)\rho_w(NIR_S)}{\rho_a(NIR_L)+t_v(NIR_L)\rho_w(NIR_L)} \end{cases}. \tag{6}$$

Then,

$$\varepsilon^{(e)}_{(NIR_S,NIR_L)} = \left[1-\frac{t_v(NIR_L)\rho_w(NIR_L)}{\rho_{rc}(NIR_L)}\right]\varepsilon_{(NIR_S,NIR_L)} + \frac{t_v(NIR_L)\rho_w(NIR_L)}{\rho_{rc}(NIR_L)}\alpha_{(NIR_S,NIR_L)}. \tag{7}$$

Therefore, $\varepsilon^{(e)}_{(NIR_S,NIR_L)}$ is the linear interpolation between $\varepsilon_{(NIR_S,NIR_L)}$ and $\alpha_{(NIR_S,NIR_L)}$ according to the weight of $t_v(NIR_L)\rho_w(NIR_L)/\rho_{rc}(NIR_L)$.

Since $t_v(NIR_S) \approx t_v(NIR_L)$, we have $\alpha_{(NIR_S,NIR_L)} \approx \rho_w(NIR_S)/\rho_w(NIR_L)$. According to the reflectance and transmittance for radiance and irradiance crossing air-water interface, there is a relationship between ρ_w and subsurface irradiance ratio R as

$$\rho_w = \frac{\pi t_s(1-\rho)(1-\tilde{\rho})R}{n_w^2 Q(1-rR)}, \tag{8}$$

where t_s is the atmospheric diffuse transmittance for irradiance from top of the atmosphere (TOA) to the sea surface; ρ is the Fresnel reflecting coefficient for upward radiance; $\tilde{\rho}$ is the mean reflecting coefficient for downward radiances; r is the subsurface reflecting coefficient for upwelling irradiance; n_w is the refraction index of water, and Q is the ratio of the upwelling irradiance and the upward radiance at the subsurface. Note that we ignore the wavelength dependence in Eq. (8). At the NIR, absorption by phytoplankton and CDOM can be neglected. According to the result of Morel and Gentili (1993) [30], we have the expression of R as follows:

$$R = f\left(\frac{0.5b_w + \tilde{b}_s b_s^* C_{\mathrm{TSM}}}{a_w + a_s^* C_{\mathrm{TSM}}}\right), \tag{9}$$

where, f is a constant depending on the angle distribution of incidence radiance and the inherent optical properties of water; a_w and b_w are the absorption and scattering coefficients of the pure seawater; C_{TSM} is the concentration of the suspended particulate matter; a_s^* and b_s^* are the specific absorption and scattering coefficients of suspended particulate matter; and

#170576 - $15.00 USD Received 13 Jun 2012; revised 13 Aug 2012; accepted 14 Aug 2012; published 24 Aug 2012

$\tilde{b}_s$ is the backscattering ratio. Since t_s, ρ, $\tilde{\rho}$, n_w, Q, b_s^* and $\tilde{b}_s$ are weakly dependent on wavelength and b_w can be neglected in turbid water, then we have

$$\alpha_{(NIR_S,NIR_L)} \approx \frac{\rho_w(NIR_S)}{\rho_w(NIR_L)} \approx \left[\frac{a_w(NIR_L)+a_s^*(NIR_L)C_{\mathrm{TSM}}-rf\tilde{b}_s(NIR_L)b_s^*(NIR_L)C_{\mathrm{TSM}}}{a_w(NIR_S)+a_s^*(NIR_S)C_{\mathrm{TSM}}-rf\tilde{b}_s(NIR_S)b_s^*(NIR_S)C_{\mathrm{TSM}}}\right]. \quad (10)$$

Based on the measurement through a tank experiment, Moore et al. (1999) [31] found that b_s^* varied from 0.032 to 0.295 m^2/g, and a_s^* varied from 0.011 to 0.022 m^2/g at 750nm. Although b_s^* is about one order larger than a_s^*, the item $rf\tilde{b}_s b_s^* C_{\mathrm{TSM}}$ is much smaller than $a_s^* C_{\mathrm{TSM}}$ due to the $rf\tilde{b}_s$ is general less than 0.005. Therefore, we can ignore the $rf\tilde{b}_s b_s^* C_{\mathrm{TSM}}$ in Eq. (10), and then

$$\alpha_{(NIR_S,NIR_L)} \approx \frac{a_w(NIR_L)+a_s^*(NIR_L)C_{\mathrm{TSM}}}{a_w(NIR_S)+a_s^*(NIR_S)C_{\mathrm{TSM}}}. \quad (11)$$

If we take the value of a_s^* as 0.015 m^2/g, then the variation of $\alpha_{(765nm,865nm)}$ with C_{TSM} is shown in Fig. 8. As C_{TSM} increases from 1.0 mg/l to 1000.0 mg/l, $\alpha_{(765nm,865nm)}$ decreases from 1.93 to 1.25. Based on both the in situ and remote sensing data, Doron et al. (2011) [32] found that $\alpha_{(765nm,865nm)}$ varied from 2 down to 1 with increasing turbidity, which was in agreement with our theoretical deduction.

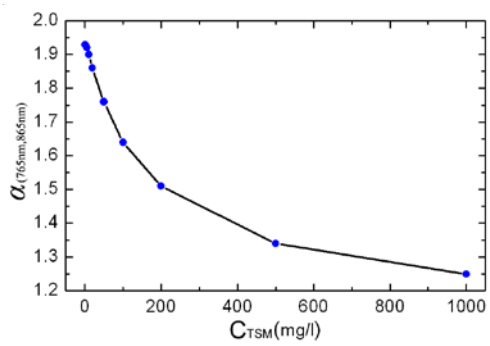

Fig. 8. Variation of $\alpha_{(765nm,865nm)}$ with the concentration of suspended particulate matter.

According to Eq. (7), since $\varepsilon_{(NIR_S,NIR_L)}$ is generally around 1.0, the value of $\varepsilon^{(e)}_{(NIR_S,NIR_L)}$ increases with C_{TSM} due to the increase of $t_v(NIR_L)\rho_w(NIR_L)/\rho_{nc}(NIR_L)$. However, when C_{TSM} is larger than a critical concentration, $\varepsilon^{(e)}_{(NIR_S,NIR_L)}$ decreases with C_{TSM} due to the decrease of $\alpha_{(NIR_S,NIR_L)}$.

The above analysis is the theoretical deduction of the variation of $\varepsilon^{(e)}_{(NIR_S,NIR_L)}$ with water turbidity, but how about the reality? Here, we calculate $\varepsilon^{(e)}_{(745nm,865nm)}$ with GOCI satellite data from 5 April 2011 (Fig. 9(a)), and also retrieve the C_{TSM} using the regional empirical algorithm developed by He et al. (subm.) [29] (Fig. 9(b)). Clearly, $\varepsilon^{(e)}_{(745nm,865nm)}$ has the lowest value in Hangzhou Bay and coasts of the Subei Shallow with extreme turbidity, while in the

#170576 - $15.00 USD Received 13 Jun 2012; revised 13 Aug 2012; accepted 14 Aug 2012; published 24 Aug 2012

mouth of Hangzhou Bay with moderate turbidity, $\varepsilon^{(e)}_{(745nm,865nm)}$ has the highest value, which is consistent with the theoretical deduction.

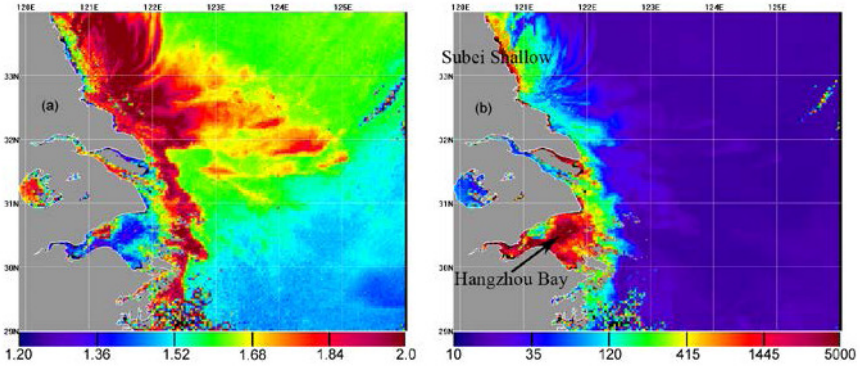

Fig. 9. $\alpha_{(745nm,865nm)}$ and C_{TSM} retrieved by GOCI data at 12:28 (Beijing time) on 5 April 2011. (a) $\alpha_{(745nm,865nm)}$, (b) C_{TSM} with unit of mg/l.

Appendix B: theoretical validation of UV-AC algorithm

For a certain band in the VIS, the aerosol scattering reflectance is

$$\rho_a^{VIS} = \rho_a^{NIR_L} \varepsilon^{(NIR_L - VIS)/(NIR_L - NIR_S)}. \tag{12}$$

However, the estimated aerosol scattering reflectance at the VIS band by the UV-AC algorithm is

$$\left(\rho_a^{VIS}\right)^{(e)} = \rho_{rc}^{UV}\left[\varepsilon^{(e)}\right]^{-(NIR_L - UV)/(NIR_L - NIR_S)} = \left(\rho_a^{UV} + t_v^{UV}\rho_w^{UV}\right)\left[\varepsilon^{(e)}\right]^{-(NIR_L - UV)/(NIR_L - NIR_S)}. \tag{13}$$

Thus, the error of the retrieved water-leaving reflectance (including the atmospheric diffuse transmittance) is

$$\begin{aligned} -\Delta\left(t_v^{VIS}\rho_w^{VIS}\right) &= \left(\rho_a^{VIS}\right)^{(e)} - \rho_a^{VIS} = \rho_a^{UV}\left[\varepsilon^{(e)}\right]^{-(NIR_L - UV)/(NIR_L - NIR_S)} + \\ & t_v^{UV}\rho_w^{UV}\left[\varepsilon^{(e)}\right]^{-(NIR_L - UV)/(NIR_L - NIR_S)} - \rho_a^{NIR_L}\varepsilon^{(NIR_L - VIS)/(NIR_L - NIR_S)}. \end{aligned} \tag{14}$$

Generally, $\varepsilon^{(e)}$ is larger than ε, therefore,

$$\begin{aligned} -\Delta\left(t_v^{VIS}\rho_w^{VIS}\right) &\le \rho_a^{UV}\varepsilon^{-(NIR_L - UV)/(NIR_L - NIR_S)} + t_v^{UV}\rho_w^{UV}\varepsilon^{-(NIR_L - UV)/(NIR_L - NIR_S)} - \\ & \rho_a^{NIR_L}\varepsilon^{(NIR_L - VIS)/(NIR_L - NIR_S)} = \rho_a^{NIR_L} + t_v^{UV}\rho_w^{UV}\varepsilon^{-(NIR_L - UV)/(NIR_L - NIR_S)} - \\ & \rho_a^{NIR_L}\varepsilon^{(NIR_L - VIS)/(NIR_L - NIR_S)}, \end{aligned} \tag{15}$$

and

$$\begin{aligned} -\Delta\left(t_v^{VIS}\rho_w^{VIS}\right) &\ge \rho_a^{UV}\left[\varepsilon^{(e)}\right]^{-(NIR_L - UV)/(NIR_L - NIR_S)} + t_v^{UV}\rho_w^{UV}\left[\varepsilon^{(e)}\right]^{-(NIR_L - UV)/(NIR_L - NIR_S)} - \\ & \rho_a^{NIR_L}\varepsilon^{(NIR_L - UV)/(NIR_L - NIR_S)} = \rho_a^{UV}\left[\varepsilon^{(e)}\right]^{-(NIR_L - UV)/(NIR_L - NIR_S)} + \\ & t_v^{UV}\rho_w^{UV}\left[\varepsilon^{(e)}\right]^{-(NIR_L - UV)/(NIR_L - NIR_S)} - \rho_a^{UV}. \end{aligned} \tag{16}$$

#170576 - $15.00 USD Received 13 Jun 2012; revised 13 Aug 2012; accepted 14 Aug 2012; published 24 Aug 2012

Since ε (or $\varepsilon^{(e)}$) is close to 1.0, and we can take the Taylor expression for ε^x (or $\left[\varepsilon^{(e)}\right]^x$) at 1.0, that is

$$\varepsilon^x = 1.0 + x\left(\varepsilon - 1\right) + \Delta. \tag{17}$$

Then, there is

$$\begin{aligned} -\Delta\left(t_v^{VIS}\rho_w^{VIS}\right) \le t_v^{UV}\rho_w^{UV}\left[1-\left(\varepsilon-1\right)\left(NIR_L - UV\right)/\left(NIR_L - NIR_S\right)\right] - \\ \rho_a^{NIR_L}\left(\varepsilon-1\right)\left(NIR_L - VIS\right)/\left(NIR_L - NIR_S\right), \end{aligned} \tag{18}$$

and

$$\begin{aligned} -\Delta\left(t_v^{VIS}\rho_w^{VIS}\right) \ge t_v^{UV}\rho_w^{UV}\left[1-\left(\varepsilon^{(e)}-1\right)\left(NIR_L - UV\right)/\left(NIR_L - NIR_S\right)\right] - \\ \rho_a^{UV}\left(\varepsilon^{(e)}-1\right)\left(NIR_L - UV\right)/\left(NIR_L - NIR_S\right). \end{aligned} \tag{19}$$

If we take the wavelengths of UV, NIR_S and NIR_L as 365nm, 765nm and 865nm, respectively, then there are

$$\begin{cases} \Delta\left(t_v^{VIS}\rho_w^{VIS}\right) \ge \rho_a^{NIR_L}\left(\varepsilon-1\right)\left(865-VIS\right)/100 - t_v^{UV}\rho_w^{UV}\left(6-5\varepsilon\right) \\ \Delta\left(t_v^{VIS}\rho_w^{VIS}\right) \le 5\rho_a^{UV}\left(\varepsilon^{(e)}-1\right) - t_v^{UV}\rho_w^{UV}\left(6-5\varepsilon^{(e)}\right) \end{cases}. \tag{20}$$

Further, we take $\varepsilon \approx 1.0$, and assume $\varepsilon^{(e)} \approx 1.2\varepsilon$, then

$$\begin{cases} \Delta\left(t_v^{VIS}\rho_w^{VIS}\right) \ge -t_v^{UV}\rho_w^{UV} \\ \Delta\left(t_v^{VIS}\rho_w^{VIS}\right) \le \rho_a^{UV} \end{cases}. \tag{21}$$

Substituting Eq. (2) into Eq. (S21), then

$$\begin{cases} \Delta\left(t_v^{VIS}L_w^{VIS}\right) \ge -\left(F_0^{VIS}/F_0^{UV}\right)t_v^{UV}L_w^{UV} \\ \Delta\left(t_v^{VIS}L_w^{VIS}\right) \le \left(F_0^{VIS}/F_0^{UV}\right)L_a^{UV} \end{cases}. \tag{22}$$

Acknowledgments

The MODIS L1B data were obtained from NASA/GSFC MODAPS Services Website. The in situ remote sensing reflectance data in the Mississippi River Estuary and Orinoco River Estuary were acquired from the SeaBASS, and we appreciate the corresponding data providers. We thank KORDI/KOSC for providing the GOCI L1B data and Dr. Zhifeng Yu for processing the MODIS data by SeaDAS. This research was supported by the National Basic Research Program of China (973 Program, grant 2009CB421202), the public science and technology research funds projects of ocean (grant 200905012), the National Natural Science Foundation of China (grants 40976110 and 40706061), and the National High Technology Research and Development Program of China (863 Program, grants 2007AA092201, 2007AA12Z137 and 2008AA09Z104). We would like to thank two anonymous reviewers for their valuable comments.